IJHSR
ijhighschoolresearch.org
RESEARCH ARTICLE

Modular Active Control System with Dual-Mode Piezoelectric Film for Reducing Satellite Solar Array Vibrations

Cayson J. Wang

The Academy of Science and Technology, The Woodlands College Park High School, 3701 College Park Dr, The Woodlands, TX 77384, USA; caysonwang@gmail.com

ABSTRACT: Satellites are crucial for the modern world, enabling internet services and telecommunication, all powered by solar panels. However, temperature changes, attitude maneuvers, and deployment impacts cause vibrations in solar panels, which can hinder accuracy, stability, and structural integrity. As the number of satellites increases exponentially, this issue will become more prevalent. Existing solutions are often bulky or consume significant power, highlighting the need for more modular and effective solutions. This paper presents a single piezoelectric film that functions in dual mode as both a sensor and an actuator, thereby reducing weight and cost. The prototype included a mockup solar panel with an embedded piezoelectric Macro Fiber Composite (MFC) film and a control circuit. The control circuit, using a microcontroller, rapidly toggled Solid-State Relays (SSR) to enable the MFC to operate in dual mode and drove the MFC to actively suppress vibrations based on a PID (Proportional-Integral-Derivative) algorithm. Data from a wireless accelerometer demonstrated vibration reduction, with a 53% decrease in root mean square (RMS) and a 54% reduction in peak-to-peak amplitude, thereby enhancing satellite stability and mitigating structural fatigue. The results demonstrated that the prototype reduced vibrations via a cost-effective and modular design.

KEYWORDS: Engineering Mechanics, Aerospace Engineering, Control Theory, Embedded Systems, Microcontrollers.

Introduction

Satellites are essential to modern life. They support communication, internet access, and broadcasting services.[1] Satellites also provide navigational services via GPS and assist in weather forecasting, environmental monitoring, and scientific research.[2] A critical component of satellites is their solar panels, which convert solar energy into electricity to power onboard systems.

One major challenge is the vibrations of these solar panels. A common cause is thermal snap - sudden temperature changes as satellites move in and out of Earth's shadow cause rapid thermal contraction and expansion, inducing vibrations.[3] Additional vibration sources include attitude maneuvers and deployment/docking impacts.[4]

These vibrations are among the top three causes of structural fatigue in satellites. They can reduce the lifespan of solar panels, degrade image resolution, and weaken communication signals. With the number of satellites rapidly increasing, addressing this issue is increasingly urgent. For instance, SpaceX's Starlink program alone plans to deploy up to 42,000 satellites into low Earth orbit by 2032.[5] To be viable for space applications, vibration control systems must be lightweight, modular, and cost-effective, as launch costs scale significantly with payload.[6]

Piezoelectric materials are widely used in active vibration control systems. The direct piezoelectric effect generates electrical charges in response to mechanical deformation, while the reverse effect induces deformation when an electrical field is applied.[7] These properties make piezoelectric materials function as either sensors or actuators. However, the direct and reverse effects cannot occur simultaneously in a single material, so traditional systems use separate piezoelectric elements for sensing and actuation.[8]

One of the project's novelties is the ability to enable a single piezoelectric material to operate in dual mode, alternating between sensing and actuation through advanced circuit design. This will reduce the piezoelectric material used in the active control system by half, thereby cutting cost and weight. A thin, flexible piezo MFC film was chosen for its lightweight and easy integration with various host structures.[9]

The goal was to demonstrate that a single MFC film controlled by a circuit with SSRs could effectively reduce vibrations by rapidly switching between sensing and actuation modes. Experimental results confirmed the prototype system's performance, achieving approximately 50% vibration reduction in a lightweight, scalable, and cost-efficient design.

Methods

To build a prototype system, a mock solar panel was constructed using a 30 in x 5 in acrylic board, clamped at one end and free at the other. This configuration allowed the panel to resonate at a frequency under 1 Hz - similar to the solar panels in space. Figure 1 illustrates the system setup for lab testing. An MFC film (Smart Material, M5628-P1) was mounted near the clamped end and connected to a custom control circuit operated by a microcontroller (Raspberry Pi Pico, RP2350). Additionally, an oscilloscope (Rigol, DS1104Z-S Plus) was used to monitor the circuit during the test, though it was not part of the prototype system.

DOI: 10.36838/IJHSR86.63

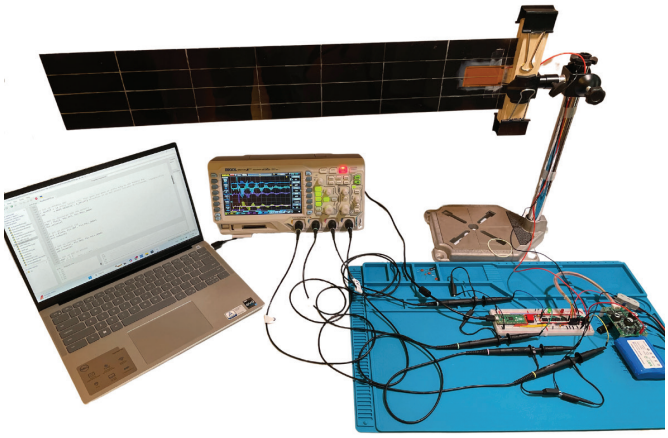

Figure 1: The system overview shows a model solar panel (30 in x 5 in x 0.08 in) with a single embedded MFC piezo film, a control circuit, and a lab test setup that includes a digital oscilloscope and a laptop. Both the laptop and the oscilloscope are for lab testing only and not part of the prototype.

The control circuit had three modes: sensing, actuation, and discharge. In sensing mode, the MFC detected vibrations and converted them into voltage signals. As shown in Figure 2, these signals were processed by the microcontroller, which then generated an actuation voltage to drive the same MFC film as an actuator, providing a counteracting force to reduce vibrations.

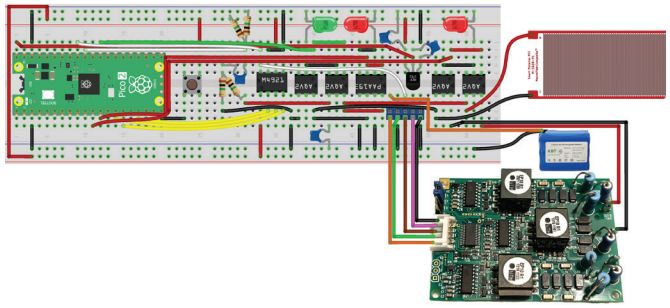

Figure 2: The circuit diagram includes a microHVA-2 power amplifier on the bottom right, a rechargeable 12 V lithium battery, and a control circuit on a breadboard. The control circuit allows the single MFC film to act as both a sensor and an actuator.

Sensing:

In sensing mode, the MFC film acted as a sensor, generating a voltage proportional to the amount of axial strain variation when the solar panel bent during vibrations. Figure 3 shows the detailed circuit design diagram. The microcontroller activated Solid State Relays (SSRs) 1 and 2 (Panasonic, AQV258), while all other SSRs remained off. SSR 1 and SSR 2 routed the MFC output through a low-pass filter (C2, 10 nF) and a voltage divider (R1 and R2 at 1 MΩ) to smooth and scale the signals. The filtered signal was then passed through a capacitor (C1, 10 μF) to remove any DC (Direct Current) offset, and a new DC bias of 1.65 V was added using a voltage divider (3.3 V source with R3 and R4, both 1 MΩ) (Figure 3). This conditioned signal fell within the input range of the microcontroller, 0-3.3 V, enabling accurate vibration sensing. A green LED 1 illuminated during sensing mode, while LEDs 2 and 3 remained off.

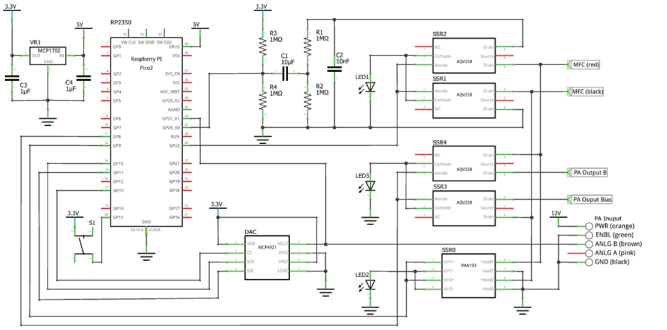

Figure 3: The control circuit diagram shows the components and pins interfacing with the MFC and the power amplifier. The microcontroller rapidly toggles certain SSRs to enable the MFC to operate in either sensing, actuation, or discharging mode to drive the MFC and actively suppress vibrations based on a PID algorithm.

Actuation:

Based on the sensed signals, the microcontroller applied a voltage to the MFC film to induce a deformation in the opposite direction of the vibrations. This voltage was calculated using a PID control algorithm, as shown in Figure 4:[10]

$$V_{out}(t) = K_p \cdot e(t) + K_i \int e(t)dt + K_d \cdot \frac{de(t)}{dt}$$

where $e(t)$ is the error between the setpoint of 1.65 V and the sensed voltage, K_p, K_i, and K_d are the proportional, integral, and derivative coefficients, respectively.

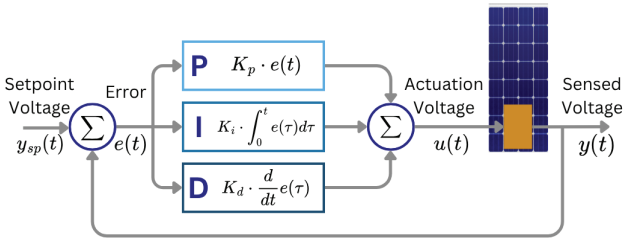

Figure 4: The PID control flowchart shows how the actuation voltage is derived from the sensed voltage using PID control theory. It's used in actuation mode, causing the MFC film to apply forces that counteract vibrations.

The PID controller is a robust closed-loop feedback mechanism widely used in industrial control systems due to its simplicity and effectiveness.[10] The controller continuously calculates an error value as the difference between a desired setpoint and the measured process variable (in this case, the sensed voltage due to the vibration of the solar panel). The PID then attempts to minimize this error by adjusting the system output based on three distinct control terms: Proportional, Integral, and Derivative. The Proportional term K_p responds to the present error, the Integral term K_i, accounts for the accumulation of past errors, and the Derivative term K_d anticipates future errors based on the current rate of change.[10] By carefully tuning these three coefficients, the PID controller can provide precise and stable control of a dynamic system, effectively dampening unwanted oscillations.

Tuning the K_p, K_i, and K_d coefficients is critical for optimal performance. While many modern tuning methods exist, the classic Ziegler-Nichols method was chosen because it is a straightforward and practical approach well-suited for this project.[11] This method involves systematically adjusting the

proportional gain K_p until continuous oscillations of the system occur (the ultimate gain, K_u), and recording the period of these oscillations, T_u. From these two empirical values, prescriptive formulas below for a standard PID were used to determine initial stable coefficients:[11]

$$K_p = 0.6 \cdot K_u,\ K_i = 1.2 \cdot \frac{K_u}{T_u},\ K_d = 0.075 \cdot K_u \cdot T_u$$

This hands-on, observational process allows for a robust starting point for the PID parameters without requiring complex mathematical modeling of the solar panel dynamics, balancing theoretical principles with experimental simplicity.

As for the implementation of the PID controller in Figure 3, because the Analog-to-Digital Converter (ADC) in the microcontroller had a unipolar range from 0 to 3.3 V, the setpoint was set at an offset of 1.65 V, corresponding to the steady state of the solar panel with no vibration. The microcontroller's digital output voltage was passed through a Digital-to-Analog Converter (DAC) (Microchip Technology, MCP4921) and was amplified 400 times by a power amplifier (Smart Material, microHVA-2). Two output pins of the power amplifier were used: Output B and the Bias pin.[12] Output B contained the resulting amplified output, and the Bias pin outputted a constant DC voltage of 500V. During actuation mode, the microcontroller switched SSR3 and SSR4 on (Panasonic, AQV258) and left all other SSRs off, thereby connecting Output B and Bias Pins to the MFC (Figure 3). The Bias pin was necessary because it allowed for both positive and negative input voltages to the MFC film, enabling it to bend forward and backward. LED 3 was on while LEDs 1 and 2 were off, indicating live actuation mode.

Discharge:

After actuation, the residual charge remained on the MFC film, which could interfere with sensing. To safely transition back to sensing mode, the MFC needed to be discharged. First, both MFC terminals were set to the same voltage. Since the MFC film was connected to the Bias pin at 500 V, the Output B pin of the power amplifier also had to output 500 V, creating a net difference of 0 V on the power amplifier outputs and discharging the MFC (Figure 3). For this to happen, the microcontroller needed to output a constant voltage of 1.25 V via the DAC to the power amplifier's analog input, because it corresponded to 500 V after being amplified by the power amplifier. Then the microcontroller turned SSR 5 (Littelfuse Inc., PAA193) on and all other SSRs off to connect both MFC terminals to the ground, bringing them to 0 V (Figure 3). A red LED 2 was on while LEDs 1 and 3 were off, indicating live discharging mode. The discharge process took about 10ms in total. After the MFC was fully discharged, it was then safe to switch to the sensing mode.

Cycling:

This system continuously cycled through sensing, actuation, and discharge modes to process active vibration control in real time. Each cycle consisted of: 20 ms sensing, 20 ms actuation, and 10 ms discharge. This allowed the MFC film to operate at a frequency of 20 Hz, effectively functioning as both a sensor and actuator in a closed-loop control system.

Testing:

The prototype was tested for its ability to reduce vibrations on the mock solar panel. Two trials were conducted: one with PID control and one without. Figure 5 illustrates a mechanical release mechanism employed to generate a consistent disturbance. A wireless accelerometer (WITMOTION, WT9011DCL) was attached to the free end of the panel to measure the vibrations.

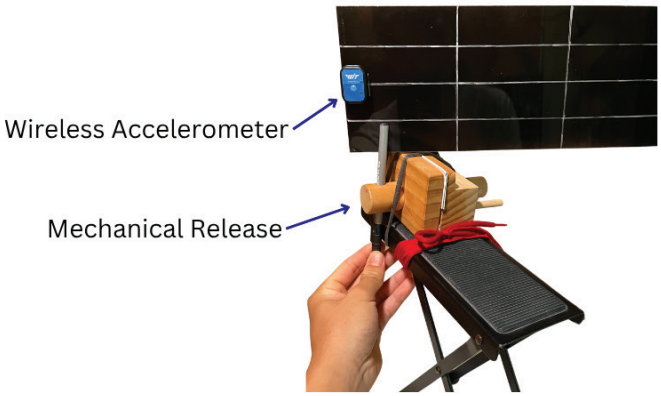

Figure 5: This figure depicts the mechanical release mechanism that provides consistent disturbance and a wireless accelerometer for data collection during the lab test. Both are only needed for testing and not part of the prototype.

In addition to the accelerometer, the MFC itself was also used to monitor vibrations. The microcontroller recorded both sensed and actuation voltages during each trial. With the microcontroller and rapid switching via SSRs, the single MFC film successfully operated in dual mode, validating its use in active vibration control. The performance of the prototype system and the experimental results further supported our hypothesis.

Results and Discussion

Results:

The prototype system was built and tested using a mock solar panel. A consistent release mechanism introduced a controlled disturbance that excited the solar panel. A wireless accelerometer was attached to the free end of the solar panel to record the vibrations. The solar panel was first excited without the use of the control system, and acceleration data was collected. Then the solar panel, under the same excitation, was dampened with the control system turned on to determine the effectiveness of reducing the vibrations. Acceleration data was collected the same way, using the wireless accelerometer. The controlled vibration data was compared against the uncontrolled vibrations. They were both plotted onto an acceleration (g) over time (s) graph in Figure 6.

DOI: 10.36838/IJHSR86.63

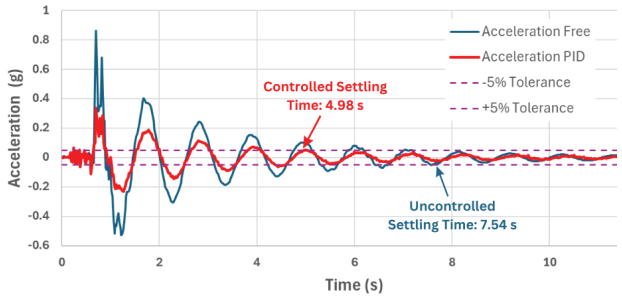

Figure 6: The accelerations recorded by the wireless accelerometer compare the controlled (in red) test vs the non-controlled (in blue) test. It indicates the effectiveness of the control system with a 34% reduction in settling time and 53% in RMS acceleration.

In Figure 6, the peak-to-peak accelerations were calculated based on the collected acceleration values. The differences between the first five crests and troughs of the acceleration values of the controlled and uncontrolled tests were compared. The controlled vibrations had a 54% reduction in average. Settling time is the duration for vibrations to fall within ±0.05 g against the final value of 0 g. It was reduced from 7.54 s (uncontrolled) to 4.98 s (controlled), a 34% improvement. The root mean square (RMS) value was used to determine how far the collected acceleration values deviated from 0 g, reflecting on the overall stability of the solar panel with and without control. The uncontrolled result had an RMS of 0.17 g, whereas the controlled test had an RMS of 0.077 g, resulting in a 53% reduction.

Figure 7 compares the voltages generated by the MFC film in sensing mode for both controlled and uncontrolled cases. This voltage corresponds to the axial strain at the clamped end of the solar panel and is directly proportional to the displacement of the free end. The controlled sensed voltage is nearly in phase with the uncontrolled sensed voltage. Conversely, the output voltage driving the MFC actuation mode is out of phase with the sensed voltage being controlled. This negative correlation confirms the effective functioning of the Proportional (P) component within the PID controller. Essentially, the MFC film senses the solar panel's deformation during vibration. The microcontroller, implementing PID control, generates an opposing voltage amplified by the power amplifier to drive the MFC film, counteracting the panel deformation and reducing vibration.

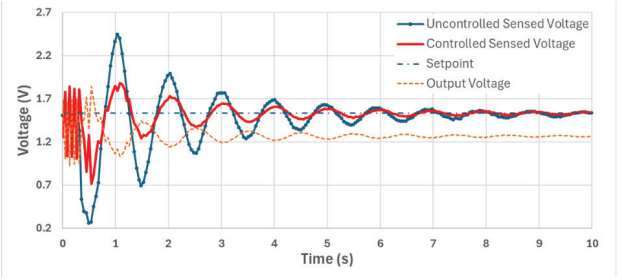

Figure 7: The voltages recorded by the MFC film in sensing mode show the voltage over time for controlled and uncontrolled vibrations. Voltage is used as a measurement of strain on the solar panel, corresponding to the vibrations it experiences. The negative correlation between the sensed voltage (red solid line) and the output voltage to drive the MFC (orange dashed line) confirms the effective functioning of the Proportional (P) component within the PID controller.

Figure 8 shows exponential curves that fit the vibration peaks, which were used to evaluate the attenuation in vibrations. The uncontrolled vibrations had an initial value of 0.77 g and a decay constant of -0.366. The controlled signal started at 0.36 g with a decay constant of -0.384, indicating faster damping.

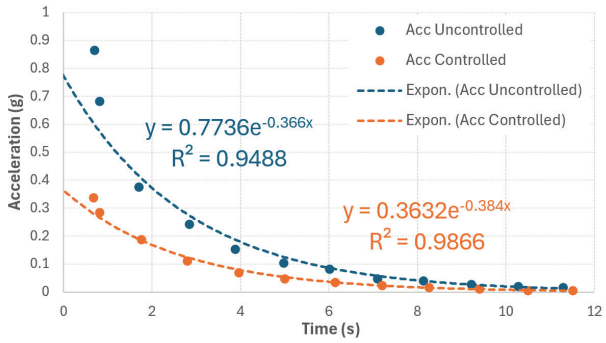

Figure 8: The exponential decay model uses curve fitting of peak accelerations for the controlled and uncontrolled vibrations. It compares the rate of decay of controlled and uncontrolled vibrations. The estimated decay constant decreased from -0.366 (uncontrolled) to -0.384 (controlled), indicating faster damping.

Discussion:

The tests using the accelerometer confirmed the effectiveness of the control system. A 54% reduction in peak-to-peak acceleration showed that the control system lowered the magnitudes of vibrations (Figure 6). The reduced peak accelerations indicated that the mock solar panel stayed closer to its setpoint when the control system was active. Additionally, the control system achieved a 53% reduction in RMS acceleration, reflecting improved stability. Enhanced stability is crucial for satellites, as it can lead to better pointing accuracy and higher image resolution. Furthermore, the control system can mitigate fatigue damage in solar panels, potentially extending their operational lifespan.

The time histories of acceleration and voltage supported these findings, as shown in Figure 7. The wireless accelerometer measured at the free end of the solar panel, while the voltage history represented axial strain variations in the MFC film attached to the clamped end. Both curves showed a similar reduction, around 50%. The strong correlation between the wireless accelerometer and MFC voltage also validated the MFC's accuracy in sensing vibrations. Thus, the control system with an embedded MFC film is capable of self-sensing, eliminating the need for an external accelerometer and further reducing weight and costs if implemented in space.

The exponential functions also confirmed the effectiveness of the control system. The linear coefficient in the exponential model for the controlled test was 0.363 - about half that of the uncontrolled case, indicating an effective reduction in initial vibration amplitude. The decay constants were -0.384 for the controlled case and -0.366 for the uncontrolled case, indicating that vibrations dampened more quickly with the control system. Additionally, both exponential models had a high R^2.

The control system also reduced the settling time by 37% further demonstrating its ability to dampen vibrations quickly. In space, this faster stabilization is beneficial in mit-

igating disturbances caused by thermal snap, docking, and attitude maneuvers. This result supported our hypothesis that a dual-mode MFC can be effective in active vibration control systems for solar panels.

Despite its compact size, the prototype system proved highly effective. The MFC film measured only 1.1 in x 2.2 in, while the model solar panel was 5 in x 30 in, making the panel 62 times larger than the area of the MFC. The combination of the MFC film and the Raspberry Pi Pico microcontroller offered a lightweight (under 60 grams), low-cost (under $250), modular, and scalable design. The control system is the first of its kind to utilize a single MFC as both a sensor and actuator, thereby significantly reducing cost and complexity. The low cost and weight of the control system will reduce large amounts of cost when mass produced, and the use of one MFC makes the system easier to monitor and maintain. By reducing vibrations, the control system could alleviate satellite failures, which can cost the industry millions of dollars per incident.[13]

The system's operating frequency may limit its effectiveness in dampening the solar panels that have a high resonant frequency. This system operated at a period of 50 ms, including 20 ms of sensing, 20 ms of actuation, and 10 ms of discharge, which corresponded to a frequency of 20 Hz. This frequency was 20 times faster than the resonant frequency of the mock solar panel (1 Hz). It was observed that the operating frequency should be at least 10 times faster than the resonant frequency of the solar panel to ensure control stability. Because the system cycled through sensing and actuation modes, the sensing duration actually added a delay to the actuation mode and induced a control error, which decreased the effectiveness of the dual-mode PID. To reduce the control error caused by this time delay, one method was to increase the operating frequency or shorten the sensing duration. However, the latency in SSRs and the microcontroller's ADC constrained the highest possible operating frequency. Therefore, the system operating frequency of 20 Hz was chosen to balance the stability and error reduction, making it 20 times faster than the solar panel's resonant frequency. The proposed solution may be suitable for the solar panels with a long wingspan that have a resonant frequency under 1 Hz. For the short-wingspan solar panels with a higher resonant frequency, such as those used in a CubeSat, the effectiveness may be hindered.

Conclusion

In conclusion, the control system is the first of its kind to utilize a single MFC as both a sensor and an actuator, offering a significant reduction in size, weight, and cost. Its modular design and proven effectiveness make it a promising solution for space and Earth applications.

While the prototype performed well on a model solar panel, scaling it for larger panels is necessary for real-world applications. The plan includes using multiple and larger MFC films to accommodate larger or hinged panels. To implement the prototype system in space, the author also intends to test the updated system in space-like conditions, such as a vacuum, microgravity, or extreme temperatures, and compare its performance to Earth-based results.

The control system has a wide range of applications, particularly for long, beam-like structures that experience low-frequency vibrations. In space, these include solar sails and wind turbines on spacecraft. On Earth, the control system could be applied to the blades of wind turbines, where vibration reduction can enhance performance.[14] It also has robotics applications, where it could help stabilize machines operating in unpredictable environments.

Acknowledgments

I truly thank my parents for their constant support during this research. I would like to thank Thomas Daue from Smart Material Corp. for providing MFC films, the power amplifier, and advice on MFC usage. I would also appreciate Rigol Technologies, Inc., providing the digital oscilloscope. Special thanks go to Dr. Naz Bedrossian and Dr. Fuh-Gwo Yuan for the insightful guidance on control theory and space applications.

References

1. *The Role of Small Satellites in NASA and NOAA Earth Observation Programs*; 2000. https://doi.org/10.17226/9819.
2. Manning, C. G. *What is a satellite? - NASA*. NASA. https://www.nasa.gov/general/what-is-a-satellite/.
3. Oda, M.; Honda, A.; Suzuki, S.; Hagiwar, Y. Vibration of satellite solar array paddle caused by thermal shock when a satellite goes through the eclipse. In *InTech eBooks*, 2012. https://doi.org/10.5772/52626.
4. Li, D.; Liu, W. Vibration control for the solar panels of spacecraft: Innovation methods and potential approaches. *International Journal of Mechanical System Dynamics* **2023**, *3* (4), 300–330. https://doi.org/10.1002/msd2.12094.
5. Witze, A. 2022 was a record year for space launches. *Nature* **2023**, *613* (7944), 426. https://doi.org/10.1038/d41586-023-00048-7.
6. Prince, F. A.; Engineering Cost Office; NASAMarshall Space Flight Center. *Weight and the Future of Space Flight Hardware Cost Modeling*. https://ntrs.nasa.gov/api/citations/20030062056/downloads/20030062056.pdf.
7. Kg, P. I. S. & Co. *Fundamentals of Piezo Technology*. Physikinstrumente. https://www.physikinstrumente.com/en/expertise/technology/piezo-technology/fundamentals.
8. Williams, D.; Khodaparast, H. H.; Jiffri, S.; Yang, C. Active vibration control using piezoelectric actuators employing practical components. *Journal of Vibration and Control* **2019**, *25* (21–22), 2784–2798. https://doi.org/10.1177/1077546319870933.
9. *NASA Invention of the Year: Controls Noise and Vibration | NASA Spinoff*. spinoff.nasa.gov. https://spinoff.nasa.gov/Spinoff2007/ip_9.html.
10. Åström, K. J. *PID Controllers*; Isa, 1995. pp. 217.
11. Libretexts. *9.3: PID tuning via classical methods*. Engineering LibreTexts. https://eng.libretexts.org/Bookshelves/Industrial_and_Systems_Engineering/Chemical_Process_Dynamics_and_Controls_(Woolf)/09%3A_Proportional-Integral-Derivative_(PID)_Control/9.03%3A_PID_Tuning_via_Classical_Methods.
12. Smart Material Corporation. *microHVA-2 User Manual*; 2020. https://smart-material.com/wp-content/uploads/2025/02/Micro-HVA-8-2-2020.pdf.
13. Sultan, N.; Groepper, P. Analyzing real cost of past orbital failures for satellite test effectiveness and insurance. *18th International*

DOI: 10.36838/IJHSR86.633

Communications Satellite Systems Conference and Exhibit **2000**. https://doi.org/10.2514/6.2000-1227.
14. Pirrung, G. R.; Grinderslev, C.; Sørensen, N. N.; Riva, R. Vortex-induced vibrations of wind turbines: From single blade to full rotor simulations. *Renewable Energy* **2024**, *226*, 120381. https://doi.org/10.1016/j.renene.2024.120381.

Author

Cayson Wang (Class of 2027) is a dedicated student researcher, ISEF Finalist, AIME Qualifier, and Eagle Scout. Besides STEM, he also competes in high school varsity baseball. Cayson plans to major in aerospace or mechanical engineering while continuing to play baseball in college. This article is based on his science fair project, which won the Houston & Texas State Science Fair awards in 2025.